Ocean Dynamics (2012) 62:31–44
DOI 10.1007/s10236-011-0489-1

Existence of eddies at crossroad of the Indonesian seas

Aditya R. Kartadikaria · Yasumasa Miyazawa · Kazuo Nadaoka · Atsushi Watanabe

Received: 2 April 2011 / Accepted: 5 August 2011 / Published online: 23 September 2011

Abstract An eddy-resolving Indo-Pacific ocean circulation model was applied to highlight the behavior of eddies throughout the Indonesian seas. The complexity of the topography and coastline at the entrance of the Makassar Strait induce an eddy-type throughflow, instead of a straightforward flow. A sill and a narrow passage in the Makassar strait creates a barrier and impedes the continuation of eddies from the Pacific ocean, but the existence of a steep deep basin (>500 m depth) between the Java and Flores seas indicates a possible area for eddies. Based on our numerical results, we described the presence of a unique eddy structure north of Lombok Island, which we designated the "Lombok Eddy" and verified it by performing a drifter release field experiment and reviewing monthly mean climatology data from the World Ocean Atlas 2001 and XBT PX2 track data. NCEP/NCAR reanalysis, satellite observation data, and mixed layer depth analysis were also used to confirm these processes. By analyzing numerical simulation results and available temperature datasets, two additional eddies were found. All eddies form primarily due to eastward local winds correlated with seasonal monsoon winds during the austral summer. These eddies vary synchronously at an interannual time scale. Together, they are referred to as the Lombok Eddy Train (LET), which affects the surface layer down to a depth of 60 m, and the intensity of the eddy system is strongly affected by mixed layer depth variability from December to February.

Keywords Lombok eddy train · Wind stress · February · Upwelling-downwelling · Cyclonic-anticyclinic

Responsible Editor: Tal Ezer

A. R. Kartadikaria (✉) · K. Nadaoka · A. Watanabe
Department of Mechanical and Environmental Informatics,
Tokyo Institute of Technology, 2-12-1 Ookayama,
Meguro-ku, Tokyo, 152-8552, Japan
e-mail: kartadikaria@gmail.com

K. Nadaoka
e-mail: nadaoka@titech.ac.jp

A. Watanabe
e-mail: watanabe.a.ah@m.titech.ac.jp

Y. Miyazawa
Research Institute for Global Change, Japan Agency
for Marine-Earth Science and Technology,
3173-25 Showamachi, Kanazawa-ku, Yokohama,
Kanagawa 236-0001, Japan
e-mail: miyazawa@jamstec.go.jp

1 Introduction

Lombok Island is located on the east side of Bali Island, and between them, there is a well-known deep, narrow strait called the Lombok Strait. This strait is one of the notable outlets of the Indonesian Throughflow (ITF), which directly connects the Indonesian seas with the Indian Ocean. Oceanic conditions around Lombok Island and other surrounding areas in the central part of Indonesia are essentially linked to regional circulation interference from the Pacific and Indian Oceans. The Indonesian archipelagos link the Pacific and Indian Oceans and play a crucial role in global ocean thermohaline circulation (Broecker 1991). Mechanisms of variability originating in the Pacific Ocean are interseasonally coordinated with a period of 50 days as a result of Rossby waves (Kashino et al. 1999; Qiu et al. 1999; Susanto et al. 2000) as well as mechanism eddies

with a timescale variability of 40 days (Masumoto et al. 2001), and an intraseasonal Mindanao current (Inoue and Welsh 1993; Lukas et al. 1996; Masumoto and Yamagata 1996), which propagates into the Celebes Sea and significantly affects variability in the northern part of the ITF. Originating from the Indian Ocean, a remotely forced coastal Kelvin wave introduces semi-annual variability (Arief and Murray 1996; Qiu et al. 1999; Susanto et al. 2000; Sprintall et al. 2000) and the 20–60-day long Madden–Julian–Oscillation (Molcard and Ilahude 1996). In the surface layer of the Lombok Strait, Susanto et al. (2007) investigated the theory that Ekman transport is correlated with El Niño events while geostrophic velocity is related to the occurrence of La Niña.

Close to Lombok Island, several stunning oceanic processes have been discovered recently. First, a sharp genetic split has been observed for the mantis shrimp that arose during the low sea level era (Barber et al. 2000). This segregation lasted until modern oceanographic conditions arose in response to the virtual *Wallace line* (Fig. 1), and the dynamics of this ocean current may support the theory. It currently represents in the presence of a sharp topographic change between the shallow Sunda and deep Sahul continental shelf, where the deep topography is part of the main route of the ITF. Second, Visser et al. (2004) and Susanto et al. (2005) noted that internal waves are generated by the existence of a sill associated with a water depth of less than 350 m in the Lombok Strait. Third, in a discussion of the ITF, it was shown that the Lombok Strait also plays a notable role as an outlet connecting the Indonesian seas and the Indian Ocean (Gordon et al. 2003; Susanto and Gordon 2005; Susanto et al. 2007). Fourth, an equatorial Kelvin wave that travels along the south coast of Java partially controls the seasonal variation of the Lombok Throughflow (Yamagata et al. 1996; Masumoto and Yamagata 1996; Arief and Murray 1996; Sprintall et al. 2000) and modulates the intraseasonal variability around Bali and the Lombok area (Qiu et al. 1999; Susanto et al. 2000). In addition from the scientific evidence of the importance of this area, a local fairytale about the Indonesian "Bermuda Triangle," known as the Masalembo triangle, has been passed from generation to generation of Indonesians. In January to March in particular (no official history recorded), many ship accidents have occurred, in spite of the fact that travel warnings are usually issued by the government. This is one reason for the scarcity of observations in February. Furthermore, there is a temporal bias in the collection of ocean data in Indonesian seas. Scientific cruises usually occur between late March and October. One of the motivations in this research is to provide clear scientific evidence of the possibility of unfavorable conditions around the Lombok Sea during the Austral summer.

The appearance of the Lombok domelike warm region did not garner much attention during the intensive International Nusantara Stratification and Transport project addressing the ITF conducted by the USA, France, the Netherlands, Australia, and Indonesia.

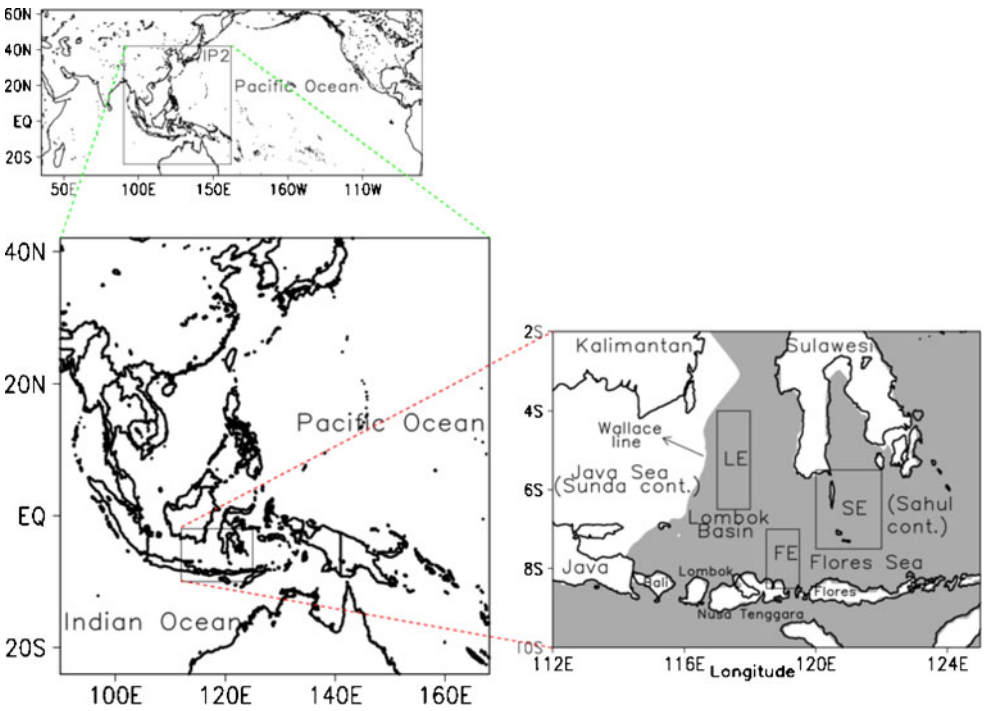

Fig. 1 The IP1 (*upper left panel*), IP2 (*lower left panel*) model domain and study interest area. Sunda and Sahul (*shaded*) shelf continental are separated by invisible line called *Wallace line* in the center of Indonesian Archipegalos. Bathymetry more than 200 m are shaded with *gray color*. *Rectangular regions* are the regions used to calculate seasonal and interannual variation. "LE," "FE," and "SE" are short of "Lombok eddy," "Flores eddy," and "South Sulawesi eddy"

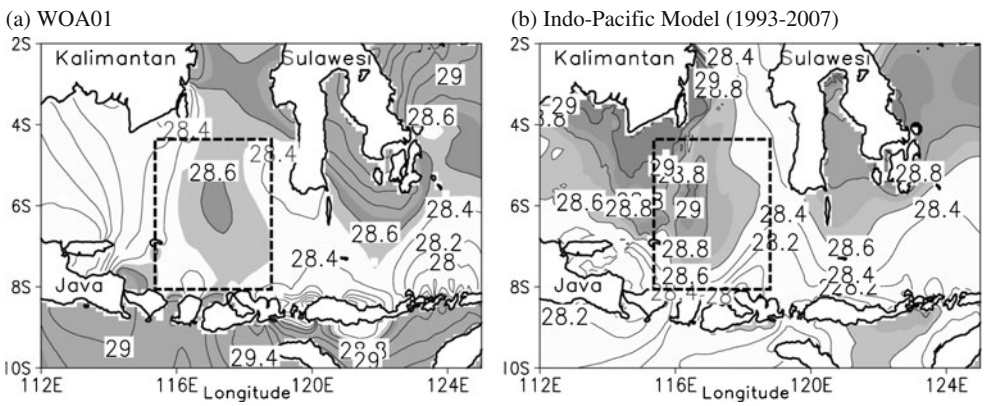

Fig. 2 February monthly mean surface temperature. **a** WOA01 and **b** IP2 model averaged 1993–2007. Contour interval is 0.2°C. Temperature at < 28.5°C are *shaded*. WOA01 is a low resolution with 1/4° while the IP2 model is 1/9° in *horizontal grid resolution*

Over 3 years of measurements in the ITF, there was no report made on eddy formation in this area, except for internal documents produced by the Indonesian Institute of Sciences (LIPI), which recorded a satellite drifter trapped in a 100-km cyclonic eddy in 1988 (Cresswell 1995). However, climatology data on temperature from the World Ocean Atlas 2001 (WOA01) show an eddy pattern to the north of Lombok Island, especially in February (dashed black box in Fig. 2a). Model results from Tozuka et al. (2001, in their Fig. 4b) showed that real-time forcing data produced increased temperatures in the south of Makassar Strait while Burnett et al. (2003) depicted a circular velocity flow between the Java and Flores Seas (in their Fig. 5). In addition, Masumoto et al. (2004) described complex circulation near the southern area of Sulawesi and proposed a further hypothesis regarding interactions between the ITF, topography, and small-scale circulation. Because the climatology and real-time forcing model show some evidence of circulation at the intersection between the Makassar Strait extension and the Java Sea, we can postulate the possibility of the existence of eddy circulation flow around this area. As this area lies to the north of Lombok Island, the term "Lombok basin" is used to describe the areas between the Java and Flores Seas. Using an eddy-resolving Indo-Pacific model, we investigated the generation, degeneration and variability of the Lombok eddy. The small islands in this area are treated very carefully, even though they do not resolve very well at a 1/9° horizontal grid resolution.

The paper is organized as follows. A brief description of the model is given in Section 2. In Section 3, the existence of eddies based on model results is discussed by examining an indicator of temperature dome structure from the available dataset. In Section 4, the generation of the Lombok eddy and other volatile nearby eddies (Flores and south Sulawesi eddy) is explained by considering seasonal variations. Here, we combine an analysis of climatology and six-hourly real-time forcing reanalysis data from the National Centers for Environmental Prediction/National Center for Atmospheric Research (NCEP/NCAR) (Kalnay et al. 1996) and QuikSCAT data. In the last section, we summarize our findings with a brief discussion.

2 Indo-Pacific model

In this research, we used an eddy-resolving numerical model that resembles a Japan Coastal Ocean Predictability Experiment (JCOPE) code developed by the Japan Agency for Marine-Earth Science and Technology (JAMSTEC). The model was based on a three-dimensional primitive-equation ocean general circulation model, known as the Princeton Ocean Model (POM), with a generalized sigma coordinate (Mellor et al. 2002). The JCOPE model succeeded in reproducing the variations of Kuroshio and mesoscale eddies in the northwestern Pacific (Kagimoto et al. 2008; Miyazawa et al. 2009a, 2005, 2008). More recently, the JCOPE model has been improved by launching the second generation of the JCOPE model, known as JCOPE2. The present version of the model can better represent finer temperature and salinity distributions with both bi-harmonic diffusion and flux-corrected transport advection schemes (Miyazawa et al. 2009b).

Here, a nested grid ocean model with a two-level nesting structure was used. The outer model encompasses most of the Indian and Pacific Oceans (62° N–30° S, 35° E–70° W) with a 20-min horizontal grid resolution and 21 vertical layers. Hereafter, the coarse outer model is known as IP1, and the high-resolution interior model is known as IP2 model (Fig. 1). IP2 covers the region around South East Asia and the West Pacific (42° N–24° S, 90° E–168° E) with a 1/9° grid resolution covering the domain model with 704 × 596 arrays with 47 vertical layers.

The monthly mean temperature and salinity (TS) of WOA01 is used for TS boundary conditions in IP1

while the elevation and velocity of the outer grid are set to zero, and we let the barotrophic mode fluctuate following radiation boundary conditions. The outer model is necessary to provide the lateral boundary values of the prognostic variables for the higher horizontal resolution IP2 model. The prognostic variables are linearly interpolated onto the boundary grid points of the fine model. We save a daily boundary value at grid points of nested models.

Combined ETOPO2v2 and GEBCO bathymetry data were applied to create topography data with additional corrections in certain shallow areas, such as the Java Sea and Philippine regions. To create a proper land/sea mask, we used GEBCO 1-min data to precisely sketch small islands, which can be depicted using the desired grid resolution.

The wind stress and surface heat flux are calculated using the six-hourly NCEP/NCAR reanalysis data (Kalnay et al. 1996) with the bulk formulae mentioned in Kagimoto et al. (2008). The downward short-wave radiation value is kept the same as in the original NCEP/NCAR. The downward penetration of short-wave radiation into the water column, based on the work of Paulson and Simpson (1977), is adopted to improve the accuracy of the sea surface temperature (SST).

Salinity at the water's surface is restored to the WOA01 monthly mean climatology level at a horizontal high resolution of 1/4° and a time scale of 30 days. Here, we set 30 days of relaxation time to induce a surface salinity flux from shallow water to the bottom. The model is then spun-up for approximately 20 years for IP1 and 5 years for IP2 from initial conditions of no motion using annual monthly mean temperatures and salinity fields obtained from the WOA01. Then, six-hourly surface forcings are applied to the model's domain as real surface forcing from October 1992 until the end of the simulation in December 2007.

For verification, we used north-south and east-west velocity components from TAO/TRITON data (http://www.pmel.noaa.gov/tao/jsdisplay/). Six points along the equator in the Pacific Ocean (147° E, 156° E, 165° E, 170° W, 140° W, and 110° W) and one point in the Indian Ocean (1.5° S and 90° E) were used to validate our IP1 model. For IP2, eight points in the western Pacific (2° N, 137° E; 0°, 147° E; 2° N, 147° E; 2°S, 156° E; 0° , 156° E; 2° N, 156° E; 5° N, 156° E; and 0°, 165° E) are used to check the accuracy of the IP2 model. However, not all of the verification results are shown here, as we only selected representative results to be considered in this paper (Fig. 3). The IP1 model shows a 49–52% correlation with observed data after the filtering process while IP2 is improved by 2–7% over IP1, even though there was no filtering process employed. These correlations apply to long observation periods (mostly more than 10 years). For the IP2 model in particular, all verification points were compared at a depth of 10 m because we focused on surface layer dynamics. Only one point (0°, 165°E) at a 100-m depth was examined deeper.

3 The existence of eddies

In this section, we describe the results of an eddy-resolving model that depicted eddy patterns at the intersection of the Java Sea, Makassar Strait, Flores Sea

(a) Validation for IP1 model at 0^0, 110^0W, 75m depth

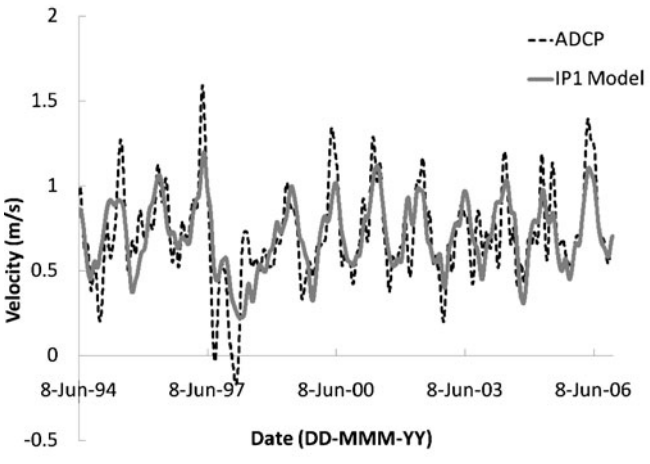

(b) Validation for IP2 model at 2^0N, 147^0E,10m depth

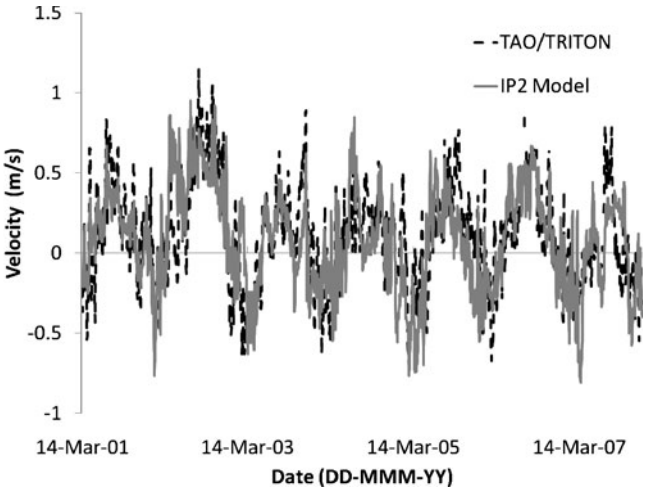

Fig. 3 One of validation results of zonal velocity component for each Indo-Pacific model. Time series for IP1 is shown on the *left figure* with 45-day filtering applied and IP2 is depicted in the *right figure* without any filtering

and Lombok Strait. We then confirmed the existence of eddies based on the results of a drifter release field experiment around the target Lombok region and examined the influence of eddies on the vertical temperature structure through verification using the available existing dataset.

3.1 Model surface dynamics and their interannual variability

The IP2 model is forced by 6-h temporal resolution, 2.5° spatial resolution NCEP/NCAR reanalysis data, which provides a good temporal resolution but low spatial resolution. For this reason, we have cross-checked the monthly climatology map with 0.1° spatial resolution QuikSCAT data for 2000–2004 (not shown). In February in particular, which is when we focus our results analysis, the higher spatial resolution QuikSCAT data showed a similar pattern of the monthly mean wind field to the results of the NCEP/NCAR data. Thus, six-hourly NCEP/NCAR reanalysis data are sufficient to represent the meteorology and surface flux conditions around the target study area in this context.

The appearance of eddies can be seen from the simulation results. These eddies are indicated with colored boxes for clarity. The dashed blue, green and red boxes in Fig. 4a correspond to the Lombok Eddy (LE), Flores Eddy (FE) and south Sulawesi Eddy (SE), respectively. These eddies are hereafter referred to as the Lombok Eddy Train (LET). Ocean circulation in February shows variation from year to year, and between the Java and Flores Seas, a basin scale of the LET is depicted. Figure 4 demonstrates the high energy level of the anticyclonic eddy, with its center occurring in the range of 6° N–7° S, 117° E–117.5° E (located around the dashed blue box). It showed that this energetic eddy varied at an interannual time scale. Another anticyclonic eddy can be seen to the south of Sulawesi (around the dashed red box). In addition, a small cyclonic eddy is seen north of Nusa Tenggara Barat Island between two anticyclonic eddies (around the dashed green box), which exhibits an unstable interannual appearance. The center of the LE does not move eastward with the Northwest monsoon wind but tends to remain around the Lombok basin. Remote effects in the Pacific may have disturbed the

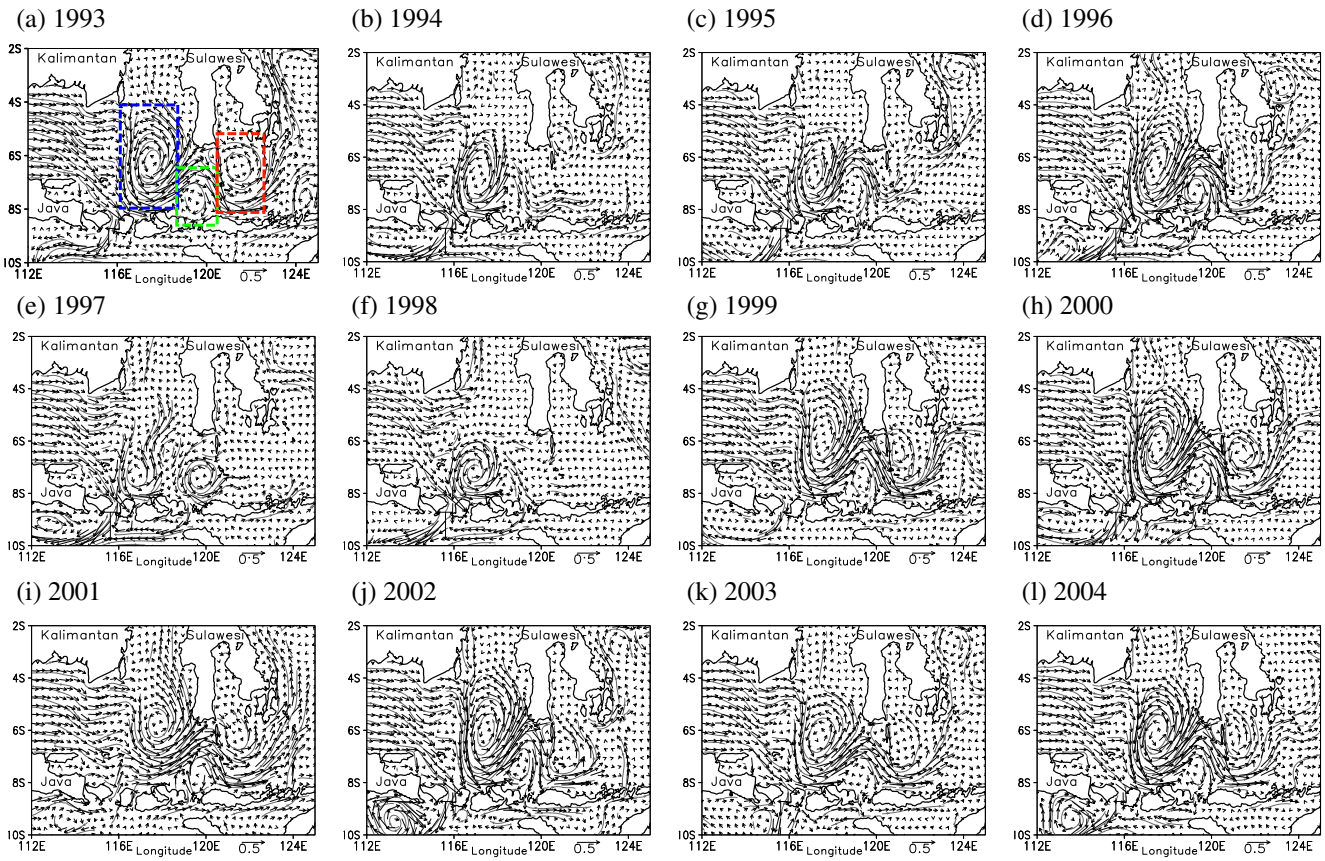

Fig. 4 Annual modeled of surface layer velocity (0–50 m) in February from 1993–2004. The contour line is a velocity stream function, and the vector unit is m/s. Lombok, Flores, and south Sulawesi eddies are denoted around *blue*, *green*, and *red box*, respectively

anticyclonic eddy during major El Niiño-Southern Oscillation events occurring from 1997–1998. During the El Niño year of 1997, the eddy did not form well, whereas during the La Niiña year of 1998, the eddy was formed, but with a smaller size. The years 1993, 1996, 1999, 2000, 2002, and 2004 showed strong formation of the LE while in 1996, 2000, 2001, and 2004, the cyclonic FE appeared. The years 1993, 1999, 2000, 2001, 2002, and 2004 exhibited strong SE formation.

3.2 Drifter release field experiment and simulation

There was no strong evidence of the eddy pattern in the Lombok sea, but this area is indicated as danger area by local governments with respect to being crossed using boats of small-medium size, especially during the Austral summer. This motivated us to conduct a cruise in mid-February 2010 to prove the existence of the LE. We released two satellite iridium drifters designed by the Zeni lite buoy Co., Ltd (http://www.zenilite.co.jp/english/). Drogues were set 10 m below the surface, and drifters reported quasi real-time positions and surface temperature every 60 min. In Fig. 5, we show that the first drifter was released close to the eastern part of the Java Sea (red dots), and the second drifter was released close to the Flores Sea (green dots). Unfortunately, the US $7,000 drifters were stolen by fishermen after 12 and 7 days for the first and second buoys, respectively. To complete the mission, we waited to release two other buoys until February 2011, when the government of Indonesia issued a travel warning regarding crossing the ocean. However, due to unfavorable sea conditions, we could not approach the target area. Still, partial success during the February 2010 cruise indicated the existence an anticyclonic eddy, where the first buoy tended to move to the southeast and the second buoy traveled slowly to the northwest.

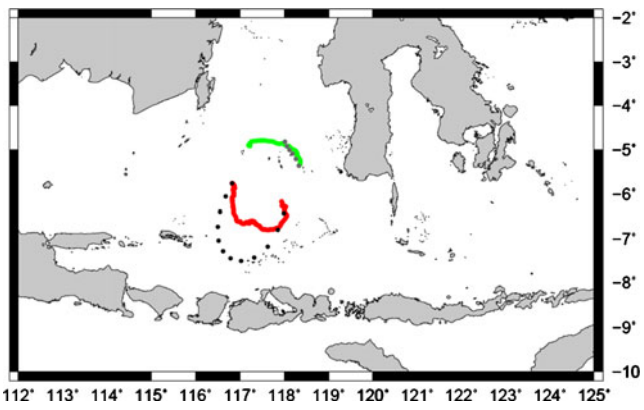

Fig. 5 The tracking pattern of the two satellite iridium drifters in 14th February 2010 (*colored dots*). Constant 10-m current drag was set to the drifters. Comparison of particle tracking simulation results were calculated and shown in *black* (*gray*) *dots* for the observed *red* (*green*) *dots* drifter. Releasing point for the first buoy (*red track*) was 6.7° S, 113.65° E, and the second buoy (*green track*) was 5.36° S, 118.34° E

We also carried out a particle tracking simulation to confirm the accuracy of our model during the field survey mission in February 2010. Lagrangian-type particle tracking was used, and a simulation was conducted during the period of the cruise mission. The modeling of particle transport is driven by the input current field. The quality of the particle trajectories is therefore limited by the quality of this current field. Components of the velocity field resulted from the hydrodynamics model conveying particle movements in three-dimensional directions. Daily averaging of elevation and velocities are used, and 1-min interpolated outputs have been applied to solve passive particle tracking. We applied a combination of 4th order Runge–Kutte (RK4) and random walk Lagrange methods to calculate new particle positions based on velocity distribution. The basic RK4 equation uses the factor $\frac{\Delta t}{6}$ instead of $\frac{\Delta t}{3}$, as shown in Eq. 1. RK4 divides time-space in the range of $x_{n+1} - x_n$ into two time steps by introducing a new variable, $x_{n+\frac{1}{2}}$. We calculate $x_{n+\frac{1}{2}}$ using a random walk Lagrange method, as shown in Eq. 2.

$$
\begin{aligned}
x_{n+1} &= x_n + \frac{1}{3}\left[k_1 + 2k_2 + 2k_3 + k_4\right] \quad \text{(a)} \\
y_{n+1} &= y_n + \frac{1}{3}\left[k_1 + 2k_2 + 2k_3 + k_4\right] \quad \text{(b)} \\
z_{n+1} &= z_n + \frac{1}{3}\left[k_1 + 2k_2 + 2k_3 + k_4\right] \quad \text{(c)}
\end{aligned}
\tag{1}
$$

where $k_1 = f(t_{n+\frac{1}{2}}, x_n) = x_{n+\frac{1}{2}} - x_n$ in x-direction, $k_2 = f(t_{k_1+\frac{1}{2}}, k_1)$, $k_3 = f(t_{k_2+\frac{1}{2}}, k_2)$, and $k_4 = f(t_{k_3+\frac{1}{2}}, k_3)$. While we calculated slopes for RK4, we inserted a calculation for a random walk Lagrange method to calculate a new position in the midpoint between t and $t + \Delta t$.

$$
\begin{aligned}
x_{n+\frac{1}{2}} &= x_n + \left[\Delta t \mathbf{U}\left(x_n\right) + d\right] \quad \text{(a)} \\
y_{n+\frac{1}{2}} &= y_n + \left[\Delta t \mathbf{V}\left(y_n\right) + d\right] \quad \text{(b)} \\
z_{n+\frac{1}{2}} &= z_n + \left[\Delta t \mathbf{W}\left(z_n\right) + d\right] \quad \text{(c)}
\end{aligned}
\tag{2}
$$

where $d = \sqrt{2A_H\Delta t}\sqrt{12}\,(R - 0.5)$ is a random walk term; A_H is kinematic viscosity; and R is a random walk number, $0 < R \leq 1$. The random walk direction is applied when particles reach the dry zone. The average of 10,000 particles released at each point is shown in black and gray dots. The particle tracking simulation described a similar type of pattern of LE,

even though the track of the first particle extended further south beyond the original 10-m observation drifter, and the track of the second particle was shorter than the observed one. However, the model can show a good agreement with the two released drifters by showing a longer distance for the first released drifter and a shorter distance for the second floater buoy.

3.3 Dome structure in observed data and model result

In this subsection, we discuss zonal transects extending from the ocean's surface to the intermediate layer. Generally, a domed temperature structure can be clearly seen in the WOA01 data, at XBT stations along the PX-2 track and in the IP2 model results (1993–2007). However, the model results showed a weaker dome structure and warmer temperatures than that in WOA01. When considering the number of data points shown at the 0.25° resolution of WOA01 in this area, a pattern can be recognized in the isotherm that can be linearly interpolated. However, the 1/4° WOA01 represents one of the most highly resolved climatologies in this area. To provide additional evidence of LET, we collected XBT data in February 1990–2011.

The zonal temperature section in February showed an upwelling region at 6.5°S,119°E between two downwelling domes at 6.5° S, 116° E, and 6° S, 121° E in both the WOA01 (Fig. 6a) and XBT PX2 track data (Fig. 6c). These two downwelling cores can be clearly observed in the WOA01 climatology data. These temperature structures are consistent with eddy patterns described previously and present good agreement with the wind stress curl explanations in the next section.

Downwelling at 116° E is associated with the location where the anticyclonic region of the LE is found. Cold water north of the Lombok islands may control the position of the west domed temperature structure. The cold water may be due to the weak positive Ekman suction associated with a negative wind stress curl, which will be discussed in the next section. Alternatively, it could be associated with the Ekman transport-induced upwelling north of Lesser Sunda that occurs during the Northwest monsoon. This western dome creates a front with the Java Sea. Downwelling also occurs south of Sulawesi at 121° E as a result of anticyclonic circulation, while upwelling nearby is caused either by the cyclonic eddy or the Ekman-induced upwelling found to the north of the Lesser Sunda Islands chain (east of Java). In general, the IP2 model forced by NCEP/NCAR reanalysis produced a weaker downwelling pattern compared with the WOA01 climatology data.

4 Eddy formation triggered by seasonal variation of local wind stress

We identify potential eddy formations by assessing possible mechanisms, observing the area of convergence and divergence in the surrounding area of the Lombok basin, and analyzing the dome structure shaped by the

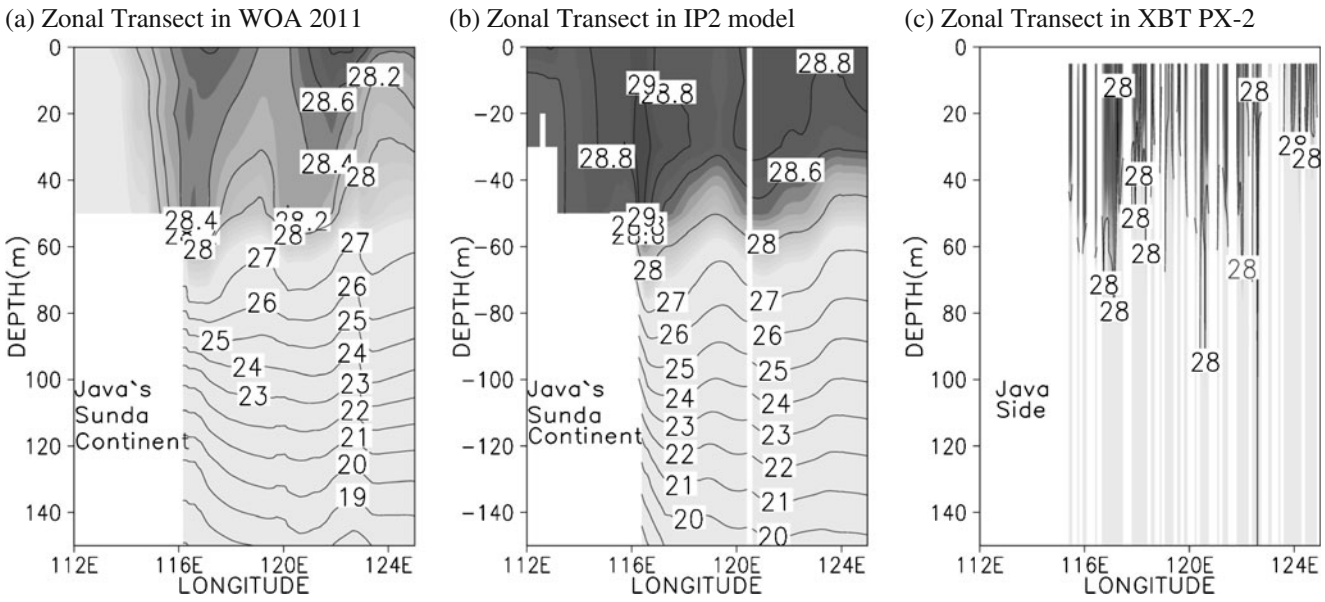

Fig. 6 Zonal vertical section from the result of **a** WOA01, **b** IP2 model, and **c** XBT PX-2 line in February averaged across 8.0°–5.5°S. Areas with temperature of > 28°C are shaded with *darker colors* and the interval is 0.2° while those with a temperature of < 28°C are marked with *light gray color* with an interval of 1°. XBT data of February were collected from 1990 to 2011

eddy. The area is not large and represents the intersection of the Java Sea, Makassar Strait, Flores Sea, and Lombok Strait. It is an area complicated by coastal upwelling signals in the northern region of the Lesser Sunda Islands (Fig. 2). We wish to reduce the strong influence of local coastal upwelling in our analysis and allow other forcing signals to appear in the domain of interest, if available.

The impact of seasonal variability in this region is greatly influenced by the Asian-Australian monsoon cycle. In this regard, many physical ocean processes show a significant response to seasonal patterns, such as the ITF, upwelling (Susanto et al. 2001), and the second mode equatorial Kelvin wave off of Java (Yamagata et al. 1996).

4.1 Local effects of the Asian-Australian monsoon season

Gordon et al. (2003) showed that external remote forcing, especially from the area of the NINO3 index in the Pacific Ocean, may control the volume of fluxes to the Indonesian seas, especially during the southeast monsoon and transition periods. However, they mentioned that during the austral summer, remote forcing is minute and suggests that strong local forcing that is dependent on other physical events. Figure 7 shows the climatology of local wind forcing between 1973 and 1993 in NCEP/NCAR data that follows the influence of monsoonal wind variability. The austral summer is characterized by a northwesterly wind while the austral winter is characterized by a southeasterly wind. It indicated that the averaged local wind (2–10° S; 112–125° E) conditions during the austral summer are significant. The magnitude is comparable with the monsoon wind during the austral winter when the external remote forcing, mentioned by Gordon et al. (2003), intensifies. Therefore, it is reasonable to take into account the effects of external local forcing in the creation of eddies in this region.

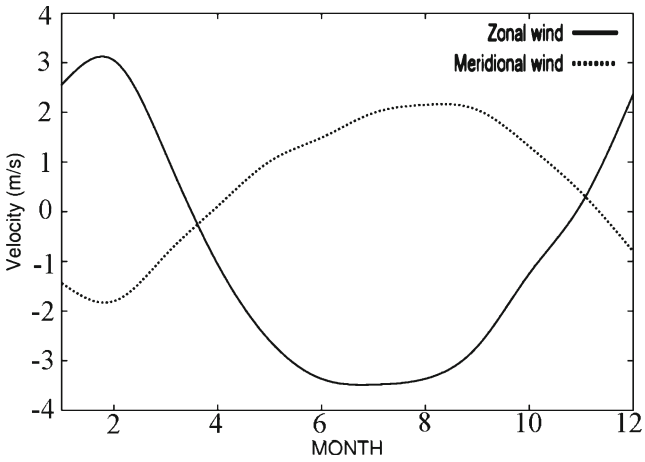

Fig. 7 Monthly mean zonal and meridional wind components on 10-m upper ocean surface. Wind analysis used six-hourly NCEP/NCAR data over the region of 10°–2° S, 112°–125° E

In general, the monsoon wind conditions during the austral summer are believed to exert the main external forcing acting in the Lombok basin area. Here, we calculated the curl of the horizontal wind stress field (Eq. 3) to measure the tendency of the wind vector field to induce rotation.

$$w = \text{curl}\,(\boldsymbol{\tau}) \tag{3}$$

Given a wind stress vector field of $\boldsymbol{\tau}\left(\tau_x, \tau_y\right)$, $w = \text{curl}\,(\boldsymbol{\tau})$ represents the rotation tendency of wind in a two-dimensional field. By calculating the Ekman pumping (Eq. 4), a similar relationship between wind stress curl and downwelling/upwelling can also be obtained. In the southern hemisphere, negative Ekman pumping ("Ekman suction"), ($w_E > 0$) indicates an upwelling process that implies cyclonic divergence.

$$w_E = \left(\frac{1}{\rho f}\left(\frac{\partial \tau_x}{\partial y}\right) - \frac{1}{\rho f}\left(\frac{\partial \tau_y}{\partial x}\right)\right) \tag{4}$$

where τ_x and τ_y are the x and y components of wind stress, $\boldsymbol{\tau}$; f is the Coriolis parameter; ρ is surface water density; and w_E is the vertical Ekman pumping velocity. In simple terms, Ekman pumping is the balance between Coriolis effects and the friction caused by the wind at the sea surface.

The open ocean of the Lombok basin clearly follows a seasonal monsoon cycle pattern (Fig. 8). In both peak monsoon seasons, February and August, the zonal monsoon wind mainly controls the pattern of the wind stress curl. During the austral summer, the area along the Makassar Strait mostly exhibits a positive curl, while the area in the open ocean of the Lombok basin presents a negative curl, also known as the Ekman convergence zone (Fig. 8a, b and l). During northwest monsoons, a relatively strong negative wind stress curl core located at 6.5° S, 120° E (right dashed red box in Fig. 8b) is concentrated around a larger weak upwelling pattern (dashed box areas in Fig. 8b), and a single strong positive wind stress curl can be found in the south of Sulawesi. In contrast, during the austral winter, a high negative curl or positive Ekman pumping can be observed in the Makassar Strait, whereas positive curls were found north of Lombok Island (Fig. 8e–i). Because of a large difference in spatial distribution of wind stress curl, we selected three boxes, as shown in Fig. 1: LE, FE, and SE, which refer to the Lombok

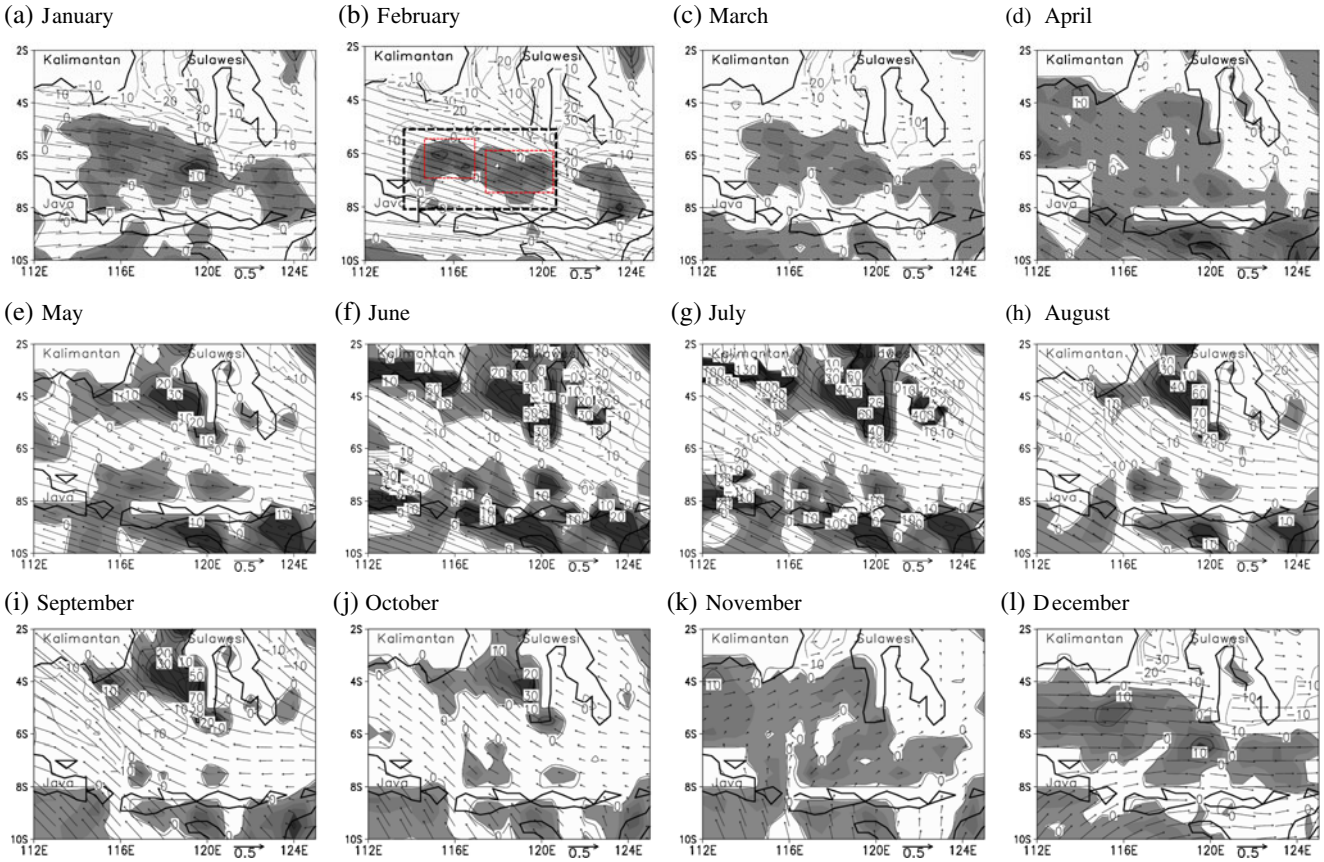

Fig. 8 Monthly climatological maps of wind stress vector (dynes/cm^2) and Ekman pumping (10^{-6}m/s). The wind stress vector is indicated with *arrow line* and Ekman pumping is contoured and shaded where upwelling (downwelling) with line/filled (*dashed line/white*). Contour interval 5×10^{-6} is used

Eddy, the Flores Eddy, and the South Sulawesi Eddy, respectively.

Because of the wide variance in the wind stress curl region, we calculated the monthly mean Ekman pumping in the boxed areas around the Lombok basin (Fig. 1). In Fig. 9a, the negative Ekman pumping velocity ($w_E < 0$)) that can be seen for the LE box in February suggests that this location is a region favorable to downwelling (convergence), even though weak upwelling associated with Ekman velocity occurs. During February, external forcing that acts on the ocean surface causes downwelling transport in the upper 60 m of the modeled water column. As a result of the forcing, an anticyclonic eddy can be formed within a box area, as we showed in a previous section. A positive curl or negative Ekman pumping in Makassar Strait contributes to formation of this downwelling, even though the negative curl-induced upwelling in the center of the Lombok basin biases this calculation. The average vertical velocity over the upper 60 m of the model shows favorable upwelling transport for the other monsoon seasons. In contrast to phenomena occurring during the austral winter, when the Ekman velocity forces downwelling, the modeled vertical velocity shows upwelling. Therefore, there is less of a chance for eddies to form during this time.

In the FE box (Fig. 9b), upwelling in February can be explained clearly because the negative wind stress curl from the derived climatological data showed the same trends inside the FE box. The model results also showed an upwelling velocity in the upper 60 m with less intensity than in the previous month. During the austral winter, the model results indicated that the downwelling pattern in the FE box of the climatological wind stress field is mainly controlled by the Ekman velocity. Interestingly, in the SE box (Fig. 9c), the phenomena occurring in February apparently differ from those in other months. However, strongly negative Ekman pumping of the climatological wind stress field only creates weak downwelling in the model results during February. This strongly negative Ekman pumping corresponds to the concentration of the positive wind stress curl in the southern Sulawesi. A stable positive wind stress curl also suggests that this

(a) Monthly mean vertical velocity of LE box

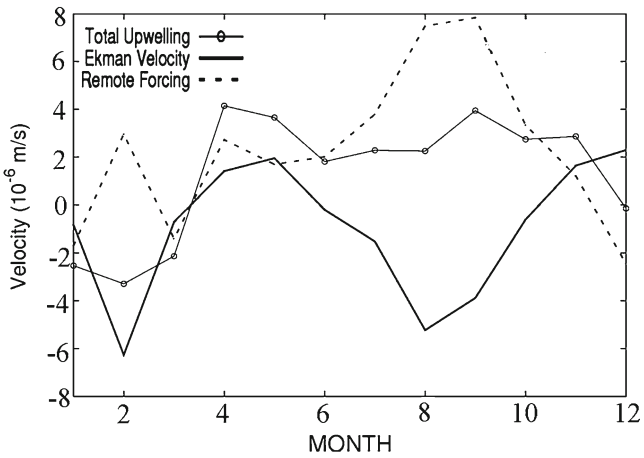

(b) Monthly mean vertical velocity of FE box

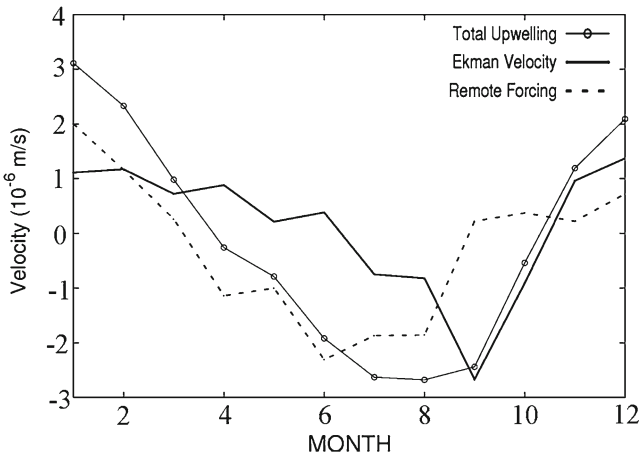

(c) Monthly mean vertical velocity of SE box

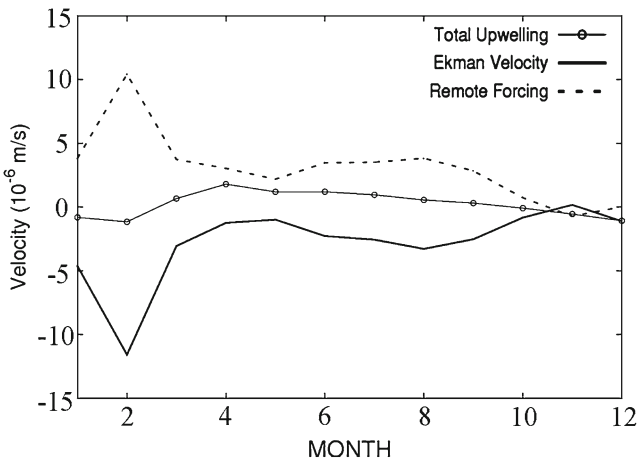

Fig. 9 Monthly mean of vertical velocity forcing calculated from boxes area in Fig. 1. The total vertical velocity calculated from upper 60-m model result and remote effect are calculated as the difference between the modeled upwelling speed (Total upwelling) and the wind-induced-Ekman pumping speed (Ekman velocity)

SE box area may exhibit a similar circulation pattern because these two locations are both dominated by the formation of downwelling. The weak magnitude of the downwelling in the SE box returned conditions to their initial state after February, which is dominated by very weak upwelling conditions in the upper 60 m. On the other hand, the negative wind stress curl core located at 6.5° S, 119° E (the FE box) might induce a small region cyclonic circulation during years of strongly negative wind stress curl.

An indication of downwelling can also be observed in the modeled isotherm and mixed layer depth results (Fig. 10). Here, mixed layer depth (h_m) is defined as the depth from the surface to a depth with a temperature of 1.0°C lower than the surface. The deeper h_m in February is also caused by the total downwelling velocity, as shown by the 27.7°C, 27.5°C, and 26.7°C isotherms, but in August, this is mainly caused by the downwelling Ekman velocity acting on the mixed layer depth or the maximum cooling of surface thermal forcing from the previous month. The isotherm graphs shown in Fig. 10 agreed with the results shown in Fig. 9a, where the total velocity triggered downwelling in February and upwelling in August but the Ekman pumping velocity created a deeper mixed layer in February and August.

The monthly AVHRR Pathfinder and weekly Multichannel Sea Surface Temperature (MCSST) satellite observation data for February can also be used to validate the February SST results of the IP2 model. In 2002, no AVHRR Pathfinder data were found for Indonesian regions while MCSST data ceased to be available in the first week of February 2001. Therefore, no comparison

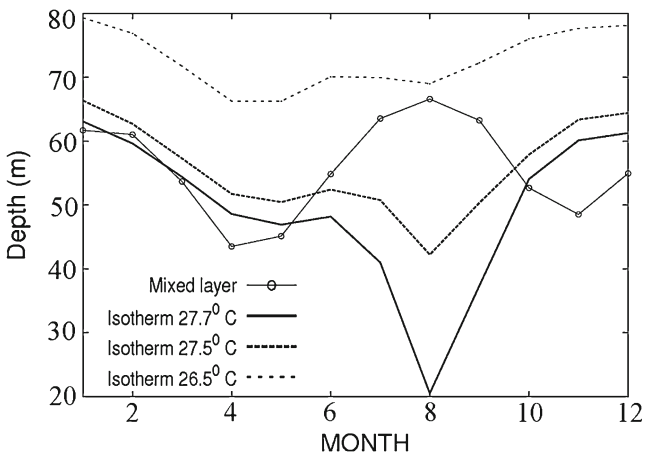

Fig. 10 The seasonal variation mixed layer depth vs. 26.5°C, 27.5°C, and 27.7°C isotherms at the Lombok basin area

data are available for February 2002. The AVHRR Pathfinder and MCSST data have 4- and 18-km spatial resolutions, respectively, and can provide a sufficient spatial resolution to validate our IP2 model. Figure 11 shows the results of the IP2 model when compared with high-resolution satellite data. The mean value is the average between nighttime and daytime, whereas the maximum and minimum deviations are the maximum and minimum values at those two times. In February 1993, the IP2 model experienced real-time forcing for the first time, causing the simulation results to exhibit far lower value than the values of the data from the two satellites. In general, the IP2 results from 1993–2000 fall between the results of the data from these two satellites. This shows that the IP2 model is sufficient for analysis of the interannual variability in February.

4.2 Testing the local wind stress curl effect

We conducted wind stress sensitivity experiments to determine the impact of the wind stress curl on the formation of the LET. We began the simulation on 17 December 2004, and we plot the monthly mean results for February 2005 in Fig. 12. The initial condition of all prognostic variables on 17 December 2004 is similar to the conditions of the normal simulation with NCEP/NCAR reanalysis data. We conducted experiments by manipulating only the wind stress components. Figure 12a is a control case, where there was no change of the wind stress applied. In Fig. 12b, the wind stress for the zonal and meridional components was set to zero throughout the IP2 domain. In Fig. 12c, the wind stress components were set to zero, except for the area between 1–11° S and 111–126° E. In that area, the normal condition of the wind stress component derived from NCEP/NCAR reanalysis data was applied. In Fig. 12d, the local wind stress was set to zero, and only the remote forcing out of domain 1–11° S, 111–126° E was set to normal wind stress conditions.

In Fig. 12b, when we set all of the wind stresses to be zero, LET disappeared. Weak and a small region circulation is found north of the Lombok islands, corresponding to a similar eddy that appears in March or April when the LET decays due to relaxed wind forcing and cooling (not shown). This small circular velocity could be associated with local topographic features. When we used normal local wind forcing conditions and set the remote wind forcing to zero, we were still able to observe the appearance of the LE. The Flores and south Sulawesi eddies coexist, but they appear hazy. Figure 12c shows that the three eddies coexist under

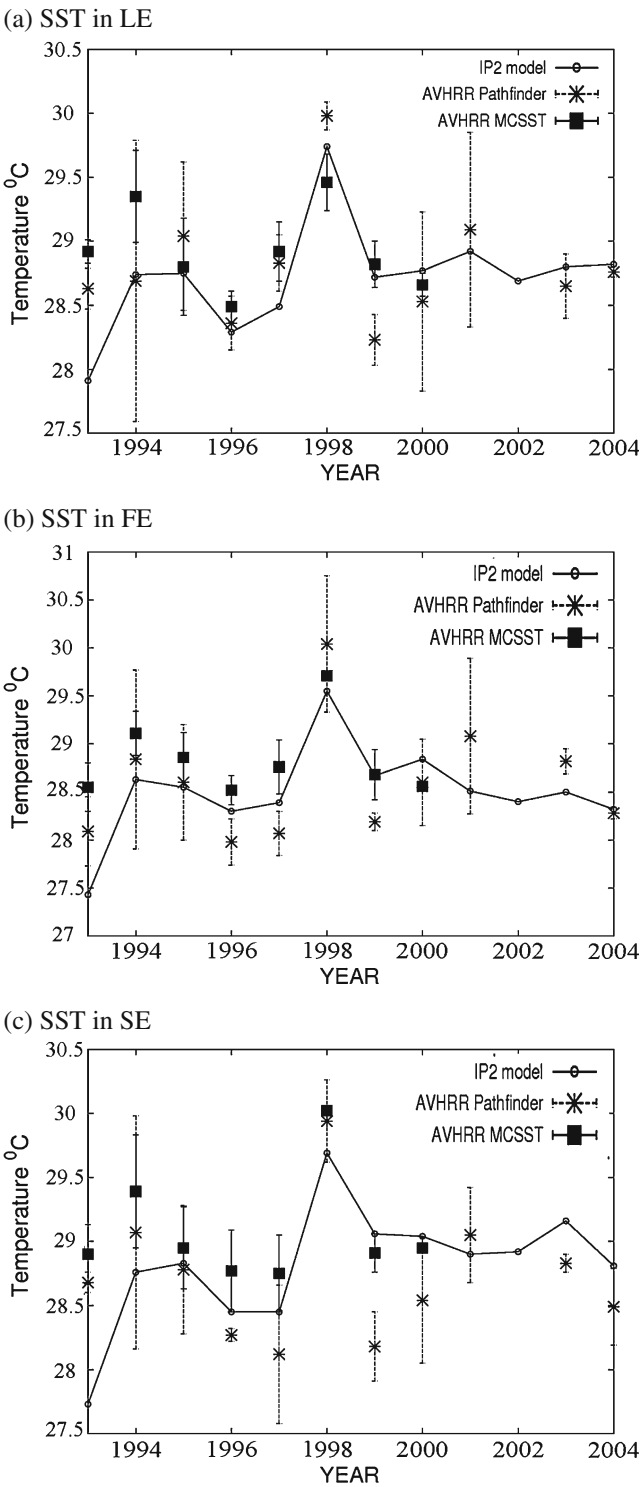

Fig. 11 SST condition in February 1993–2004 from IP2 model (*connected circles*) result, February monthly AVHRR Pathfinder (*crossed*) and February weekly average Multichannel Sea Surface Temperature (*MCSST*) 1993–2000 (*black box*) satellite observation data for **a** LE, **b** FE, and **c** SE boxes. The *error bars* denote the maximum and minimum values recorded in the daytime and nighttime from the satellite observation data. The year 2002 shows no Pathfinder data within the Indonesian region

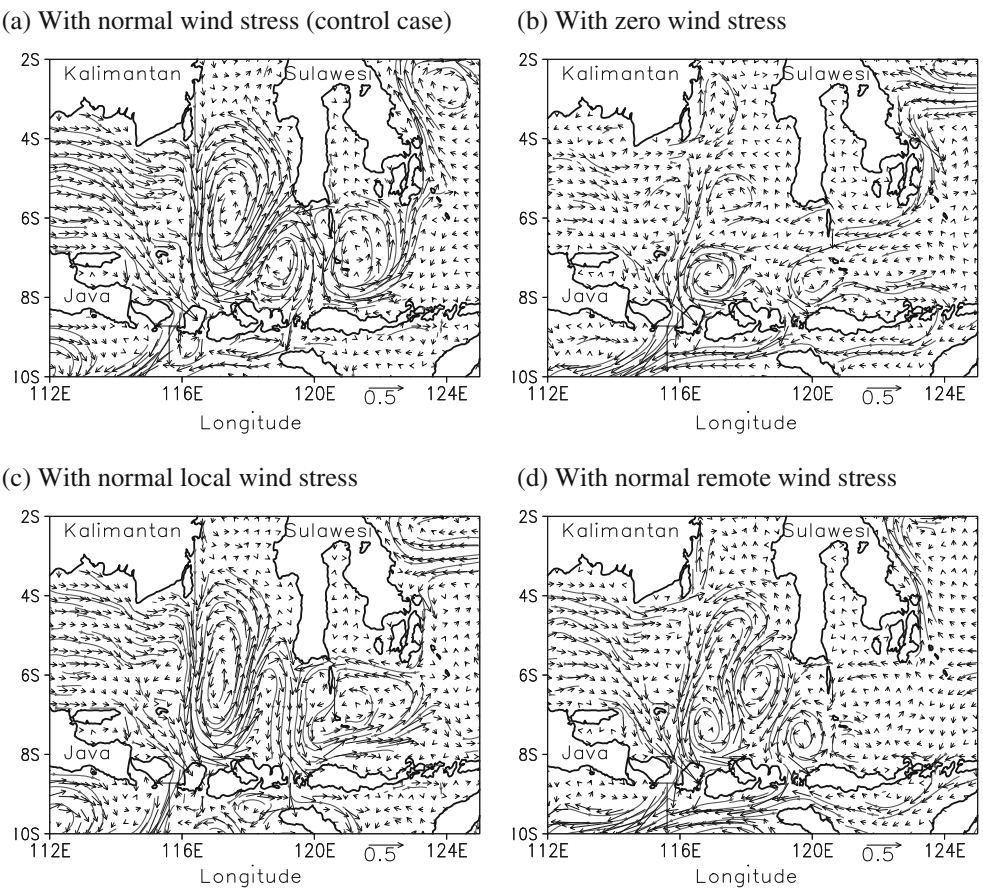

Fig. 12 Sensitivity test of wind stress term for the region affected by the LET in February 2005. Local area is defined as an area 2° larger than Fig. 1 (1–11° S, 111–126° E). Subfigure (**a**) is a control case where normal condition of wind stress is applied to local and remote area (entire IP2 domain). Subfigure (**b**) shows a condition with zero wind stress in IP2 domain (no wind stress curl) while (**c**) shows a normal condition of wind stress in local area, but zero in remote area. In contrast to (**c**), subfigure (**d**) shows a normal condition of wind stress in remote area but zero in local area

the local wind stress conditions. Here, we can conclude that the existence of the LE is dominated by local wind factors, whereas the variability of the Flores and south Sulawesi eddies may be controlled by remote wind forcing. In Fig. 12d, when we keep the normal wind stress conditions in all domains of the IP2 model but set the wind stress to zero around the LET, it can be observed that the basic structure of the LE appears, though it does not form well. The spatial scale of the eddies is shrinking, and eddy instability is depicted. A combination of anticyclonic and cyclonic eddies can be observed around the LE area. From this experiment, we can conclude that local wind forcing is important in generating the LET, and remote wind forcing is important in stabilizing the existence of the LET.

5 Conclusions

The existence of stable eddies at the beginning of the route of the ITF, such as the Mindanou dome, the Halmahera eddy and the Celebes eddy, led us to several hypotheses regarding the process associated with the generation and variability of the LET. We found that the generation process is more associated with local wind forcing, while variability appears at the interannual time scale and could be affected mostly by remote wind forcing. The LET eddy system can be observed during the austral summer when ITF transport is low. Furthermore, the complexity of the topography within the Indonesian seas is believed to trigger more complex ITF-type flows within the Indonesian region. Considering these facts, it is difficult to believe that there no mesoscale/basin eddies occur within Indonesia itself.

In this study, we examined the possibility of the existence of eddies, especially the LE, within Indonesian seas using a high-resolution eddy-resolving ocean circulation model: the Indo-Pacific2 (IP2) Model. The LE seen in the Lombok basin is generated by various mechanisms, including the development of wind stress curl and the influence of the convergence area. However, its generation is mainly triggered by an eastward wind component in February that flows almost parallel to the Lesser Sunda Islands chain. This eddy system affects the water surface below a depth of 50–70 m. A high divergence from Makassar and positive Ekman transport from the north of the Lesser Sunda Islands adjusts to the generation of water mass accumulation

in the Lombok basin. The upwelling region found to the east of the LE may represent a key origin of mass transport for the convergence comprising the Ekman-induced upwelling in the LE region. This water mass accumulation shapes an anticyclonic eddy pattern that deepens the mixed layer and thermocline. However, this eddy is not long lived. The end of the austral summer in March and April reduces the magnitude of the wind stress curl, which may lead to the decay of the LE.

The results shown in Figs. 4 and 8 suggest that other eddies may exist in addition to the LE; the unstable Flores cyclonic eddy is centered at 7.5° S, 119° E, exhibiting relatively colder temperatures, is associated with a negative wind stress curl favorable to upwelling and is further intensified by coastal upwelling north of the Lesser Sunda Islands chain during the northwesterly monsoon wind season. A warm water region south of Sulawesi may be correlated with a positive wind stress curl and may favor weak downwelling, which is intensified in the northwesterly monsoon wind season and creates the south Sulawesi anticyclonic eddy. The formation of this eddy could be triggered by the spread of 'flake' islands over this area. Finally, these three eddies (i.e., LE, FE, and SE) function as the LET system, as illustrated in Fig. 13, which varies synchronously at an interannual time scale (Fig. 4).

This system of eddies enriches physical phenomena within the Indonesian archipelagos, especially during the austral monsoon season. One possible role of this system may be influencing the distribution of pelagic organisms. Thus far, an invisible *Wallace line* has strongly affected the distribution of flora and fauna between the Sahul and Sunda continental shelf, and furthermore, a genetic break has been proven to exist for marine organisms at the geological time scale. However, there is no evidence for shorter time scale ecosystem segregation due to the Lombok eddy or LET.

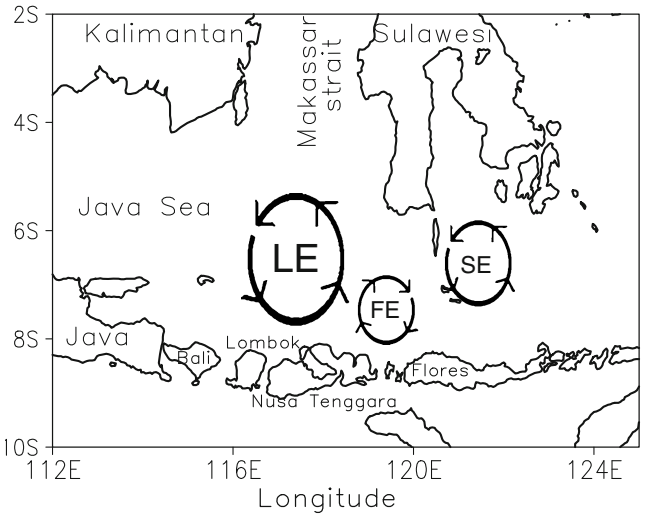

Fig. 13 The schematic picture of the Lombok eddy train in February. LE is relatively stable and depicts strong anticyclonic eddy. A volatile FE forms a cyclonic eddy pattern and favorable upwelling while SE forms an anticyclonic eddy pattern and located in the warm region in south of Sulawesi

Acknowledgments This work was funded by the Global Environment Research Fund (F-082) of the Ministry of the Environment, Japan, and a Grant-in-Aid for Scientific Research (A) (no. 18254003 and no. 21254002) from the JSPS (Japan Society for the Promotion of Science). The authors gratefully acknowledge the joint research cooperation, help, and support from the Research Center for Oceanography-Indonesian Institute of Sciences, directed by Prof. Suharsono, and the Research Center for Marine and Coastal Resources-Ministry of Marine Affairs and Fisheries of Indonesia, directed by Dr. Budi Sulistiyo. The authors gratefully acknowledge the support from Novi S. Adi and Adi Purwandhana during drifters release experiment. We benefited considerably from facilities offered by the JAMSTEC Yokohama office, which supported all of the running processes on their two supercomputers (SX-8R and SGI Altix4700) and provided time-series validation data. The Indo-Pacific code uses the code of JCOPE2 developed by the JCOPE group. The first author has been supported by the scholarship for foreign students offered by the Ministry of Education, Culture, Sports, Science and Technology (MEXT), Japan. The authors gratefully acknowledge the useful comments and suggestions from the weekly JCOPE group meeting and the anonymous reviewers.

References

Arief D, Murray SP (1996) Low-frequency fluctuations in the Indonesian throughflow through Lombok Strait. J Geophys Res 101(C5):12455–12464

Barber PH, Palumbi SR, Erdmann MV, Moosa MK (2000) A marine Wallace's line? Nature 17; 406(6797):692–693

Broecker WS (1991) The great ocean conveyor. Oceanography 4:79–89

Burnett WH, Kamenkovich VM, Gordon AL, Mellor GL (2003) The Pacific/Indian Ocean pressure difference and its influence on the Indonesian Seas circulation: part I-the study with specified total transports. J Mar Res 61; 5:577–611

Cresswell G (1995) A cyclonic eddy north of Lombok. Mar Res Indones 29:13–17

Gordon AL, Susanto RD, Vranes K (2003) Cool Indonesian throughflow as a consequence of restricted surface layer flow. Nature 425(6960):824–828

Inoue M, Welsh SE (1993) Modeling seasonal variability in the wind-driven upper-layer circulation in the Indo-Pacific region. J Phys Oceanogr 23:1411–1436

Kagimoto T, Miyazawa Y, Guo X, Kawajiri H (2008) High resolution Kuroshio forecast system—description and its applications. In: Ohfuchi W, Hamilton K (eds) High resolution numerical modeling of the atmosphere and ocean. Springer, New York, pp 209–234

Kalnay E, Kanamitsu M, Kistler R, Collins W, Deaven D, Gandin L, Iredell M, Saha S, White G, Woolen J, Zhu Y, Chelliah M, Ebisuzaki W, Higgins W, Janowiak J, Mo KC, Ropelewski C,

Wang J, Leetma A, Reynolds R, Jenne R, Joseph D (1996) The NCEP/NCAR 40-year reanalysis project. Bull Am Meteorol Soc 77:437–471

Kashino Y, Watanabe H, Herunadi B, Aoyama M, Hartoyo D (1999) Current variability at the Pacific entrance of the Indonesian Throughflow. J Geophys Res 104(C5):11021–11035

Lukas R, Yamagata T, McCreary JP (1996) Pacific low-latitude western boundary currents and the Indonesian throughflow. J Geophys Res 101:12209–12216

Masumoto Y, Yamagata T (1996) Seasonal variations of the Indonesian throughflow in a general ocean circulation model: Pacific low-latitude western boundary currents and the Indonesian throughflow. J Geophys Res 101:12287–12294

Masumoto Y, Kagimoto T, Yoshida M, Fukuda M, Hirose N, Yamagata T (2001) Intraseasonal eddies in the sulawesi sea simulated in an ocean general circulation model. Geophys Res Lett 28(8):1631–1634

Masumoto Y, Sasaki H, Kagimoto T, Komori N, Ishida A, Sasai Y, Miyama T, Motoi T, Mitsudera H, Takahashi K, Sakuma H, Yamagata T (2004) A fifty-year eddy-resolving simulation of the world ocean. Preliminary outcomes of OFES (OGCM for the Earth Simulator). J Earth Simulator 1:35–56

Mellor GL, Hakkinen S, Ezer T, Patchen R (2002) A generalization of a sigma coordinate ocean model and an intercomparison of model vertical grids. In: Pinardi N, Woods JD (eds) Ocean forecasting: conceptual basis and applications. Springer, Berlin, pp 55–72

Miyazawa Y, Yamane S, Guo X, Yamagata T (2005) Ensemble forecast of the Kuroshio meandering, 2005. J Geophys Res 110:C10026. doi:10.1029/2004JC002426

Miyazawa Y, Kagimoto T, Guo X, Sakuma H (2008) The Kuroshio large meander formation in 2004 analyzed by an eddy-resolving ocean forecast system. J Geophys Res 113:C10015. doi:10.1029/2007JC004226

Miyazawa Y, Kagimoto T, Guo X, Sakuma H (2009a) The Kuroshio large meander formation in 2004 analyzed by an eddy-resolving ocean forecast system. J Geophys Res 113:C10015. doi:10.1029/2007JC004226

Miyazawa Y, Zhang R, Guo X, Tamura H, Ambe D, Lee J-S, Okuno A, Yoshinari H, Setou T, Komatsu K (2009b) Water mass variability in the western North Pacific detected in a 15-year eddy resolving ocean reanalysis. J Oceanogr 65:737–756

Molcard R, Ilahude AG (1996) The Indo-Pacific throughflow in the Timor Passage. J Geophys Res 101:12411–12420

Paulson CA, Simpson JJ (1977) Irradiance measurements in the upper ocean. J Phys Oceanogr 7:952–956

Qiu B, Mao M, Kashino Y (1999) Intraseasonal variability in the Indo-Pacific Throughflow and the regions surrounding the Indonesian Seas. J Phys Oceanogr 29:1599–1618

Sprintall J, Gordon AL, Murtugudde R, Susanto RD (2000) A semiannual Indian Ocean forced Kelvin wave observed in the Indonesian seas in May 1997. J Geophys Res Oceans 105(C7):17217–17230

Susanto RD, Gordon AL (2005) Velocity and transport of Indonesian throughflow in Makassar Strait. J Geophys Res 110:C01005. doi:10.1029/2004JC002425

Susanto RD, Gordon AL, Sprintall J, Herunadi B (2000) Intraseasonalvariability and tides in Makassar Strait. Geophys Res Lett 27:1499–1502

Susanto RD, Gordon AL, Zheng Q (2001) Upwelling along the coasts of Java and Sumatra and its relation to ENSO. Geophys Res Lett 28(8):1599–1602

Susanto RD, Mitnik L, Zheng Q (2005) Ocean internal waves observed in the Lombok Strait. Oceanography 18(4): 80–87

Susanto RD, Gordon AL, Sprintall J (2007) Observation and proxies of the surface layer throughflow in the Lombok Strait. J Geophys Res 112(C3):C03S92. doi:10.1029/2006JC003790

Tozuka T, Kagimoto T, Masumoto Y, Yamagata T (2001) Simulated multiscale variations in the western tropical pacific: the Mindanao Dome revisited. J Phys Oceanogr 32:1338–1359

Visser WP, van Groesen E, Andonowati A, van Beckum FPH, Klopman G (2004) On the generation of internal waves in Lombok Strait through Kelvin-Helmholtz instability. MSc, thesis Applied Mathematics, Department of Applied Mathematics, University of Twente

Yamagata T, Mizuno K, Masumoto Y (1996) Seasonal variations in the equatorial Indian Ocean and their impact on the Lombok throughflow. J Geophys Res 101(C5):12465–12473